ChemComm

COMMUNICATION

View Article Online
View Journal

Cite this: DOI: 10.1039/d2cc04677f

Received 23rd August 2022,
Accepted 23rd October 2022

DOI: 10.1039/d2cc04677f

rsc.li/chemcomm

A redox-active Mn(0) dicarbene metalloradical†

Ageliki Karagiannis, [a] Alexei M. Tyryshkin, [b] Roger A. Lalancette, [a] Denis M. Spasyuk, [c] Asmaa Washington [a] and Demyan E. Prokopchuk *[a]

We report a rare redox-active Mn^0 metalloradical $[Mn(CO)_3(Ph_2B(^{tBu}NHC)_2)]^-$ (NHC = N-heterocyclic carbene) with counter-cations $[K(2.2.2)crypt]^+$, $[Na(2.2.2)crypt]^+$, or $[Li(DME)(12\text{-crown-}4)]^+$ (DME = 1,2-dimethoxyethane), all characterized *via* single crystal X-ray diffraction. Cyclic voltammograms reveal solvation-dependent $Mn^{I/0}$ redox potentials that are modeled using the Born equation.

There is ongoing interest in developing redox active transition metal complexes for applications in molecular electrocatalysis using Earth-abundant metals such as Ni, Fe, and Co.[1,2] An equally attractive metal is manganese and several groups have reported Mn^I complexes that are electrocatalytically active for CO_2 reduction to CO[3–6] and H^+ to H_2[7] *via* intermediates with a formal Mn^{-I} oxidation state. A key Mn^0 intermediate is typically proposed, however observing and chemically separating the mononuclear species has proven to be challenging because Mn^0 complexes readily dimerize to form a Mn–Mn bond, such as in $Mn_2(CO)_{10}$ and $[Mn(CO)_3(tmbp)]_2$[8] (tmbp = 4,4′5,5′-tetramethyl-2,2′biphosphinine). Likewise, $[Mn^I(CO)_3(bis\text{-}^{Me}NHC)Br]$[3] and $[Mn^I(CO)_3(^tBu\text{-}bpy)Br]$[5] (NHC = N-heterocyclic carbene, bpy = bipyridine) suffer from an off-cycle dimerization pathway during the reduction CO_2 to CO in the presence of exogenous acid. In 2014, Kubiak and co-workers used 6,6′-dimesityl-2,2′-bipyridine to increase the steric bulk of their $[Mn(CO)_3(bpy)Br]$[6] framework, which prevented dimerization.

Despite the importance of Mn^0 intermediates in small molecule activation and electrocatalysis, only a few structurally characterized monomeric Mn^0 complexes have been published to date (Fig. 1). Figueroa and co-workers reported that the incorporation of two sterically encumbering isocyanide ligands allows the formation of the monoradical $[Mn(CO)_3(CNAr^{Dipp2})_2]$,[9] an analogue to the unstable $[Mn(CO)_5]$ monoradical (Dipp = 2,6-diisopropylphenyl), demonstrating atom abstraction and radical scavenger reactivity. Deng and co-workers reported that the inclusion of NHC and alkene ligands gave rise to three-coordinate Mn^0 complexes $[(NHC)Mn(dvtms)]$,[10] which are reactive towards H_2 and unsaturated C–C bonds to yield Mn^{II} dialkyl compounds. Furthermore, Tonzetich and coworkers showed that chemical reduction of the Mn^I pyrrole-based pincer complex, $[Mn(CO)_2(^{tBu}PNP)]$, yields the mononuclear low spin Mn^0 metalloradical $[K][Mn(CO)_2(^{tBu}PNP)]$.[11] Cyclic voltammetry and treatment of $[K][Mn(CO)_2(^{tBu}PNP)]$ with $NO_{(g)}$ revealed a facile re-oxidation to the Mn^I precursor, demonstrating the robust nature of this $Mn^{I/0}$ redox couple ($E_{1/2}$ = −2.14 V *vs.* $Fc^{+/0}$, THF). We recently reported a redox-active tricarbonylmanganese(0) anion radical containing a pyrrolidine-functionalized indenyl

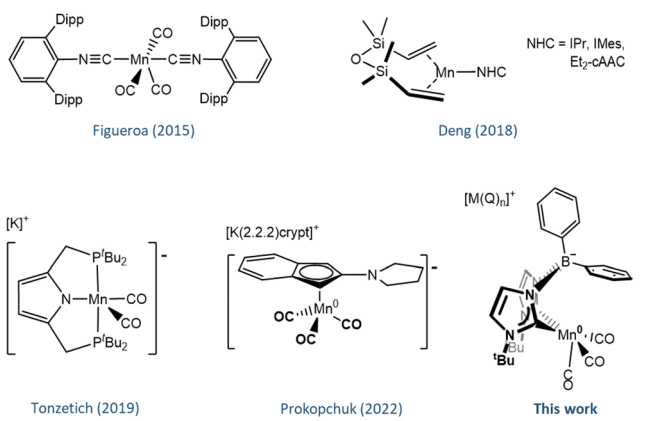

Fig. 1 Reported Mn^0 complexes in the literature and the novel Mn^0 dicarbene metalloradical. Dipp = 2,6-diisopropylphenyl, IPr = 1,3-bis(2,6-diisopropylphenyl)imidazol-2-ylidene, IMes = 1,3-bis(2,4,6-trimethylphenyl)imidazol-2-ylidene, cAAC = cyclic alkylamino carbene. $[M(Q)_n]^+$ denotes counteraction M^+ and encapsulating agent Q.

[a] *Department of Chemistry, Rutgers University – Newark, Newark, New Jersey 07102, USA. E-mail: demyan.prokopchuk@rutgers.edu*
[b] *Department of Chemistry and Chemical Biology, Rutgers University, Piscataway, NJ 08854, USA*
[c] *Canadian Light Source, Saskatoon, Saskatchewan, S7N2V3, Canada*

† Electronic supplementary information (ESI) available. CCDC 2203153–2203156. For ESI and crystallographic data in CIF or other electronic format see DOI: https://doi.org/10.1039/d2cc04677f

ligand ($E_{1/2}$ = −2.34 V *vs.* $Fc^{+/0}$, MeCN) where the aminoindenyl group exhibits partial η^5–η^3 "ring slip" character but retains its aromaticity in the solid state.[12]

We now describe the synthesis of a rare five-coordinate manganate(0) tricarbonyl complex coordinated to a borate-bridged bis(NHC) ligand that exhibits medium-dependent redox behavior. Starting with a Mn^I precursor, the singly reduced Mn^0 species can be accessed *via* cyclic voltammetry or by using alkali metal sources to generate mononuclear manganates. X-Ray crystallographic analysis confirms the molecular structure of these distorted trigonal bipyramidal complexes and the spectroscopic properties at Mn remain independent of the encapsulated counterion after crystallization ($[K(2.2.2)crypt]^+$ *vs.* $[Na(2.2.2)crypt]^+$ *vs.* $[Li(DME)(12\text{-crown-4})^+]$; DME = 1,2-dimethoxyethane).

The Mn^I complex $[Ph_2B(^{tBu}NHC)_2Mn(CO)_3]$ (**1**) is synthesized from the lithium carbene $[Li(Ph_2B(^{tBu}NHC)_2{\cdot}Et_2O]$[13] and half an equivalent of the bromide-bridged dimer $[Mn(CO)_3(^tBuCN)Br]_2$[14] with mild heating (Scheme 1, top). Formation of **1** is sensitive to the Mn source - using $MnBr(CO)_5$ was unsuccessful, mirroring observations made by Smith and co-workers for chelation of a borate-bridged tris(NHC) ligand to Mn.[14] Notably, washing the crude product with methanol is essential to remove all traces of LiBr from the product. After workup, red-orange **1** is obtained in 42% yield and was further characterized by single crystal X-ray diffraction (Scheme 1, right). The distance between the Mn atom and arene C_{ipso} atom above the metal center ($Mn\cdots C_{ipso}$ = 2.618(2) Å) is significantly longer than the sum of the Mn–C covalent radii (2.12 Å)[15] but shorter than the sum of their van der Waals radii (3.75 Å).[16]

Computational analysis (DFT) reveals bonding interactions between the *ipso* and *ortho* carbons of the arene π-system on the ligand, as portrayed in HOMO−6 and HOMO−8 (Scheme 1, bottom). This type of stabilizing interaction is expected because the coordinatively unsaturated Mn center would have only 16 valence e^- in the absence of overlap with the π-electron system of the aromatic ring. Solid-state IR spectroscopic data of **1** show

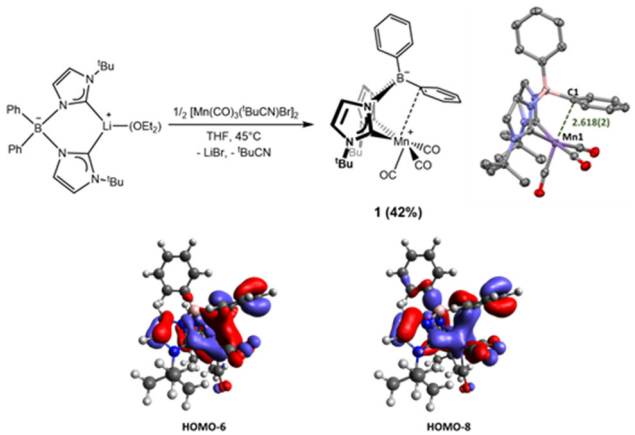

Scheme 1 Top: Synthesis of **1** and its molecular structure. $Mn\cdots C_{ipso}$ = 2.618(2) Å, 50% probability ellipsoids. Hydrogen atoms are omitted for clarity. Bottom: HOMO−6 and HOMO−8 of **1** (TPSS-D3(BJ)/def2-TZVP/CPCM(MeCN); isosurface value = 0.04; see the ESI† for additional details).

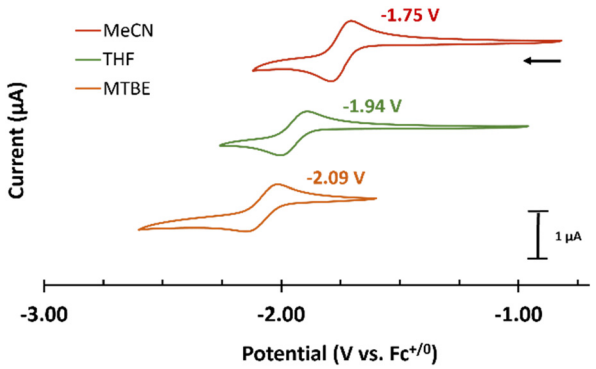

Fig. 2 CV of **1** under three different conditions: MeCN, 0.1 M $[^nBu_4N][PF_6]$ (red); THF, 0.1 M $[^nBu_4N][PF_6]$ (green); MTBE, 0.075 M $[^nBu_4N][B(C_6F_5)_4]$ (orange). In all cases, CVs were conducted under N_2 with 1 mM analyte at a scan rate of 0.1 V s^{-1}.

CO stretches at 2010, 1928, and 1881 cm^{-1} which remain identical in solution-phase IR spectroscopy in both MeCN and DCM, indicating that the Mn–arene interaction is not disrupted by solvent (Fig. S4, ESI†). Furthermore, UV-vis spectra in CH_2Cl_2 and CH_3CN only show minor differences in molar absorptivity (Fig. S12 and S13, ESI†). The observed carbonyl stretches are significantly lower than $[Mn(CO)_3(^tBuCN)Br]_2$ (2025, 1936, and 1915 cm^{-1}) but similar to those found in the methylene-bridged dicarbene complex $[Mn(CO)_3(bis\text{-}^{Me}NHC)Br]$ (2004, 1912, and 1881 cm^{-1}).[3]

Cyclic voltammograms (CVs) of **1** were conducted under N_2 to examine its solution phase electrochemical activity. CVs in anhydrous MeCN and THF reveal redox events at $E_{1/2}$ = −1.75 V and $E_{1/2}$ = −1.94 V *vs.* $Fc^{+/0}$, respectively (Fig. 2). The anodic shift on going from MeCN to a different solvent can be estimated using a modified Born equation[17,18] where $\Delta\Delta G^\circ$ is expressed in kcal mol^{-1}, z is the ionic charge (−1), ε is the dielectric constant (ε_{THF} = 7.43, ε_{MeCN} = 35.7),[19] r_{eff} is the effective spherical ionic radius in Å, and 166 is a grouping of all other constants (eqn (1)). The r_{eff} is estimated to be 5.3 Å based on distances measured from X-ray structural data for the Mn^0 anion (see below).

$$\Delta\Delta G^\circ\ (\text{solv}-\text{MeCN}) = 166\frac{z^2}{r_{eff}}\left(\frac{1}{\varepsilon_{solv}}-\frac{1}{\varepsilon_{MeCN}}\right) \quad (1)$$

Using eqn (1), we estimate $\Delta\Delta G^\circ$(THF–MeCN) = −3.3 kcal mol^{-1}, or ΔE° = 0.15 V, which is in excellent agreement with the observed potential difference of 0.19 V in Fig. 2. In addition, CV experiments with varying THF : MeCN ratios show a gradual shift in redox potential between these two extremes (Fig. S11, ESI†). To further validate this interpretation, CVs of **1** in methyl *tert*-butyl ether (MTBE) saturated with $[^nBu_4N][B(C_6F_5)_4]$[20] reveal that $E_{1/2}$ = −2.09 V *vs.* $Fc^{+/0}$. Assuming that $\varepsilon_{MTBE} \cong \varepsilon_{Et_2O}$ (4.24),[19] $\Delta\Delta G^\circ$(MTBE–MeCN) = −6.5 kcal mol^{-1} and ΔE° = 0.28 V which also agrees with experiment (ΔE° = 0.34 V). Therefore, the anion becomes more reducing as the dielectric constant decreases due to poorer solvent stabilization of the electrogenerated anion at the solution-electrode interface.

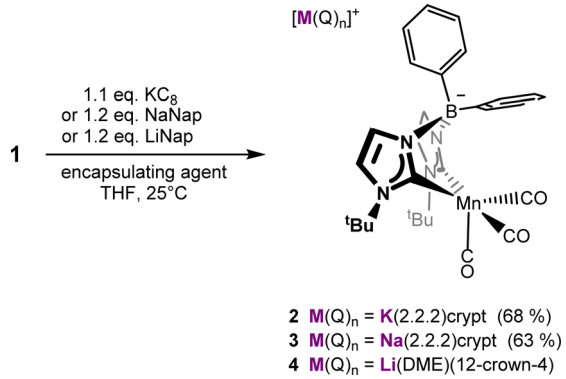

Scheme 2 Syntheses of **2**, **3**, and **4**.

We sought to chemically reduce **1** by screening its reactivity with alkali metals. Red-orange **1** can be reacted with a slight excess of KC_8, NaNap, or LiNap (Nap = naphthalenide) in THF at 25 °C to afford dark forest-green solutions. The addition of (2.2.2)crypt or 12-crown-4 yielded the crystalline green salts [K(2.2.2)crypt][Ph_2B(^{tBu}NHC)$_2$Mn(CO)$_3$] (**2**), [Na(2.2.2)crypt][Ph_2B-(^{tBu}NHC)$_2$Mn(CO)$_3$] (**3**), and [Li(DME)(12-crown-4)][Ph_2B-(^{tBu}NHC)$_2$Mn(CO)$_3$] (**4**; Scheme 2).

Complexes **2**, **3** and **4** have been characterized by single crystal X-ray diffraction and exhibit very similar structural features at the manganate ion (Fig. 3). The Mn···C_{ipso} distance increases by approximately 0.860 Å (**2**), 0.765 Å (**3**), and 0.637 Å (**4**) when compared to **1** due to increased electronic repulsion between the metalloradical and ligand (Table 1). Furthermore, there is a weak interaction between the carbonyl oxygen (OB) and potassium (K2) atoms of **2** (2.963(4) Å; Fig. 3) whereas for **3** and **4** there are no interactions between the encapsulated cation and CO ligands. A solid-state CO···[K(2.2.2)crypt]$^+$ interaction has been previously observed in a tricarbonylrhenium-bound quinoxaline salt (CO···K = 2.900(5) Å) but in the analogous manganese salt no interaction was observed.[21] A similar interaction was also observed when metallic rubidium was used as the reductant in the presence of (2.2.2)crypt to give an interatomic CO···Rb distance of 3.126(2) Å between the terminal oxygen atom and rubidium cation.[21]

Solid-state IR spectra of **2**, **3**, and **4** reveal nearly identical CO stretching frequencies that are all shifted 100–120 cm^{-1} lower than **1**, confirming the strong π backdonation effects upon reduction and that the counterion has little influence on the electronic structure at Mn (Table 1). UV-vis spectroscopy of **2** reveals a strong absorption maximum at 360 nm (ε_{360} = 1000 ± 100 M^{-1} cm^{-1}), complementary to its perceived green colour (Fig. S14, ESI†).

Solution-phase magnetic susceptibility of **2** (2.06 μ_B, Evans' method)[22] confirms the presence of one unpaired electron (S = 1/2). The electron paramagnetic resonance (EPR) spectrum of **2** (Fig. 4, left) demonstrates a rhombic symmetry with the simulation parameters g = [2.018, 2.023, 1.998] and A(^{55}Mn) = ±[212, 149, 126] MHz. One g-factor component g_z = 1.998 is close to a free electron g-factor while two other components $g_{x,y}$ are slightly larger, as expected for 3d^7 Mn^0 in a strong square-pyramidal ligand field with the unpaired spin residing on the 3d$_{z^2}$ orbital.[23,24] The EPR parameters of **2** are noticeably different from other reported square-pyramidal Mn^0 complexes, like $Mn(CO)_5$ ($g_\perp$ = 2.038, $g_\parallel$ = 2.000; $A(^{55}Mn) = [A_\perp = -94, A_\parallel = 185]$ MHz)[25] and [((*n*-Bu)$_3$P)$_2$–Mn(CO)$_3$] ($g_\perp$ = 2.036, $g_\parallel$ = 2.007; A(^{55}Mn) = [$A_\perp$ = −114, $A_\parallel$ = 164] MHz),[23] reflecting a different ligand field strength and coordination symmetry of the dicarbene ligand in **2** as compared to the CO and phosphine ligands in

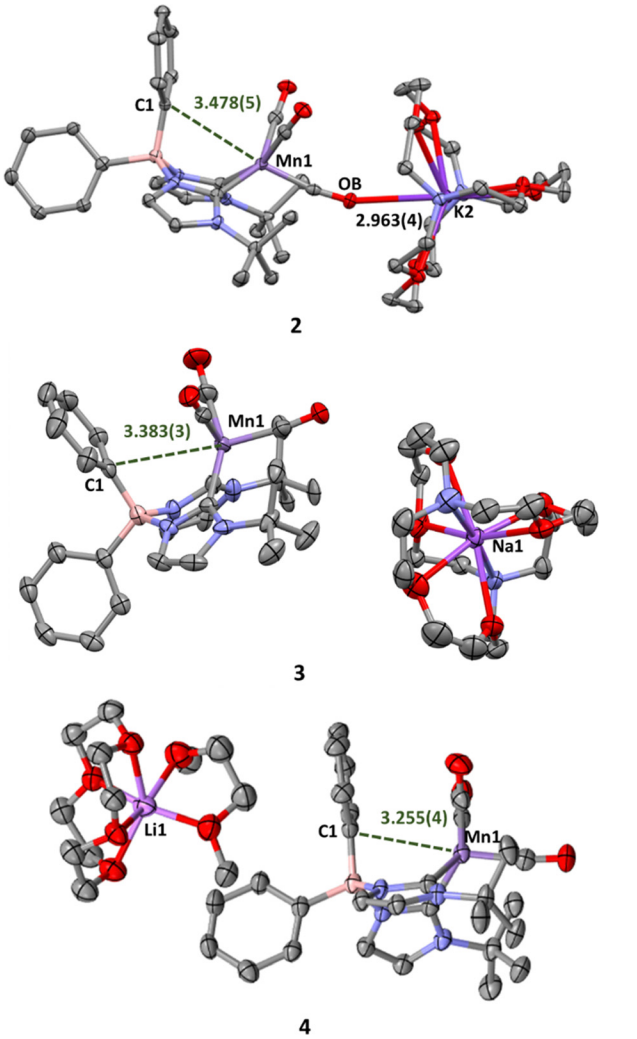

Fig. 3 Molecular structures of **2**, **3**, and **4** with 50% probability ellipsoids; H atoms omitted for clarity. Cocrystallized solvent and additional molecules in the asymmetric unit of **4** are also omitted for clarity.

Table 1 Selected bond distance comparisons and IR carbonyl stretches observed

Complex	C≡O bond distance (Å)	Mn···C_{ipso} (Å)	C≡O stretches (cm^{-1})
1	1.150(3), 1.151(3), 1.161(3)	2.618(2)	2010, 1928, 1881
2	1.166(5), 1.179(5), 1.174(6)	3.478(5)	1908, 1808, 1765
3	1.168(5), 1.166(5), 1.174(5)	3.383(3)	1908, 1801, 1771
4	1.165(6), 1.165(6), 1.165(6)	3.255(4)	1905, 1801, 1764

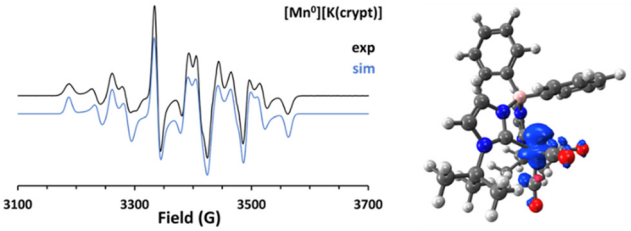

Fig. 4 Left: X-band EPR spectrum of **2** (77 K, 2-MeTHF glass): experiment (black) and stimulation (blue). Right: Computed spin density plot of the Mn^0 radical anion $\mathbf{2}^-$ at the TPSS-D3(BJ)/def-TZVP/CPCM(THF) level of theory, revealing predominantly $3d_{z^2}$ spin localization (blue) consistent with the EPR data.

the above examples. Furthermore, a high hyperfine anisotropy, as observed in **2** and the above examples, is a signature feature of a Mn^0 redox state, distinguishing it from the Mn^{II} redox state with a low hyperfine anisotropy. The pronounced rhombicity of both g and $A(^{55}Mn)$ in **2** indicates a low symmetry coordination geometry (C_{2v} or lower), promoting a sizeable admixture of $3d_{x^2-y^2}$ to the dominant $3d_{z^2}$ population.[24] The DFT-calculated spin density for **2** (Fig. 4, right) supports the predominately $3d_{z^2}$ metal-based radical character of the Mn^0 centre.

In summary, new anionic Mn^0 complexes have been synthesized from a redox-active Mn^I precursor using the chemical reductants KC_8, NaNap, or LiNap. All compounds have been structurally authenticated by single crystal X-ray diffraction and characterized by various spectroscopic methods to evaluate their structural and electronic properties. The arene ring of the borate-bridged bis(N-heterocyclic carbene) ligand plays an important role in stabilizing the Mn^I centre. The solvent-dependent redox behaviour can be rationalized using the Born equation, showing that media with a lower dielectric constant destabilize the manganate anion in solution. Upon $1e^-$ reduction, an increase in $Mn^0\cdots C_{ipso}$ distance by 0.6–0.9 Å is observed and the low spin ($S = 1/2$) Mn^0 complexes exhibit metal-based radical character, as confirmed by EPR spectroscopy and DFT calculations. The stoichiometric and electrocatalytic reactivity of this novel metalloradical complex with small molecules is ongoing.

This research was supported by a Rutgers-Newark startup grant and the Rutgers Office of Advanced Research and Computing (OARC). The authors thank Dr. Pavel Kucheryavy (Rutgers-Newark) for NMR assistance.

Conflicts of interest

There are no conflicts to declare.

Notes and references

1 R. Francke, B. Schille and M. Roemelt, *Chem. Rev.*, 2018, **118**, 4631–4701.
2 E. S. Wiedner, A. M. Appel, S. Raugei, W. J. Shaw and R. M. Bullock, *Chem. Rev.*, 2022, **122**, 12427–12474.
3 F. Franco, M. F. Pinto, B. Royo and J. Lloret-Fillol, *Angew. Chem., Int. Ed.*, 2018, **57**, 4603–4606.
4 M. Bourrez, F. Molton, S. Chardon-Noblat and A. Deronzier, *Angew. Chem., Int. Ed.*, 2011, **50**, 9903–9906.
5 J. M. Smieja, M. D. Sampson, K. A. Grice, E. E. Benson, J. D. Froehlich and C. P. Kubiak, *Inorg. Chem.*, 2013, **52**, 2484–2491.
6 M. D. Sampson, A. D. Nguyen, K. A. Grice, C. E. Moore, A. L. Rheingold and C. P. Kubiak, *J. Am. Chem. Soc.*, 2014, **136**, 5460–5471.
7 M. D. Sampson and C. P. Kubiak, *Inorg. Chem.*, 2015, **54**, 6674–6676.
8 F. Hartl, T. Mahabiersing, P. Le Floch, F. Mathey, L. Ricard, P. Rosa and S. Záliš, *Inorg. Chem.*, 2003, **42**, 4442–4455.
9 D. W. Agnew, C. E. Moore, A. L. Rheingold and J. S. Figueroa, *Angew. Chem., Int. Ed.*, 2015, **54**, 12673–12677.
10 J. Cheng, Q. Chen, X. Leng, Z. Ouyang, Z. Wang, S. Ye and L. Deng, *Chem*, 2018, **4**, 2844–2860.
11 A. L. Narro, H. D. Arman and Z. J. Tonzetich, *Organometallics*, 2019, **38**, 1741–1749.
12 D. S. Tresp, H. Neugebauer, S. Grimme, A. Hansen and D. E. Prokopchuk, *Organometallics*, 2022, DOI: 10.1021/acs.organomet.2c00463.
13 I. V. Shishkov, F. Rominger and P. Hofmann, *Organometallics*, 2009, **28**, 3532–3536.
14 A. P. Forshaw, R. P. Bontchev and J. M. Smith, *Inorg. Chem.*, 2007, **46**, 3792–3794.
15 B. Cordero, V. Gómez, A. E. Platero-Prats, M. Revés, J. Echeverría, E. Cremades, F. Barragán and S. Alvarez, *Dalton Trans.*, 2008, 2832–2838.
16 S. S. Batsanov, *Inorg. Mater.*, 2001, **37**, 871–885.
17 D. E. Richardson, *Inorg. Chem.*, 1990, **29**, 3213–3217.
18 P. Atkins and J. D. Paula, *Atkins' Physical Chemistry*, W. H. Freeman and Company, New York, 8th edn, 2006.
19 J. R. Rumble, Physical Constants of Organic Compounds, *CRC Handbook of Chemistry and Physics*, CRC Press/Taylor & Francis Boca Raton, FL, 103rd edn, 2022.
20 R. J. LeSuer and W. E. Geiger, *Angew. Chem., Int. Ed.*, 2000, **39**, 248–250.
21 S. Choua, J.-P. Djukic, J. Dalléry, A. Bieber, R. Welter, J.-P. Gisselbrecht, P. Turek and L. Ricard, *Inorg. Chem.*, 2009, **48**, 149–163.
22 D. F. Evans, *J. Chem. Soc.*, 1959, 2003–2005.
23 G. B. Rattinger, R. L. Belford, H. Walker and T. L. Brown, *Inorg. Chem.*, 1989, **28**, 1059–1066.
24 B. R. McGarvey, *Can. J. Chem.*, 1975, **53**, 2498–2511.
25 J. A. Howard, J. R. Morton and K. F. Preston, *Chem. Phys. Lett.*, 1981, **83**, 226–228.

